International Journal of Greenhouse Gas Control 108 (2021) 103317

Contents lists available at ScienceDirect

International Journal of Greenhouse Gas Control

journal homepage: www.elsevier.com/locate/ijggc

An automated system for continuous monitoring of CO_2 geosequestration using multi-well offset VSP with permanent seismic sources and receivers: Stage 3 of the CO2CRC Otway Project

Roman Isaenkov [a,b,*], Roman Pevzner [a,b], Stanislav Glubokovskikh [a,b], Sinem Yavuz [a,b], Alexey Yurikov [a,b], Konstantin Tertyshnikov [a,b], Boris Gurevich [a,b], Julia Correa [c], Todd Wood [c], Barry Freifeld [d], Michael Mondanos [e], Stoyan Nikolov [e], Paul Barraclough [b]

[a] Curtin University, Department of Exploration Geophysics, 26 Dick Perry Avenue, Kensington, WA, 6151, Australia
[b] CO2CRC, 11 – 15 Argyle Place South, Carlton, VIC, 3053, Australia
[c] Lawrence Berkeley National Laboratory, 1 Cyclotron Road, MS 74R-316C, Berkeley, CA, 94720, USA
[d] Class VI Solutions, Inc., 711 Jean St., Oakland, CA, 94610, USA
[e] Silixa Ltd., Silixa House, 230 Centennial Park, Centennial Avenue, Elstree, Hertfordshire, WD6 3SN, UK

ARTICLE INFO

Keywords:
Distributed acoustic sensors
Permanent reservoir monitoring
Time-lapse seismic
Repeatability
Seismic orbital vibrators

ABSTRACT

A permanent automated continuous seismic CO_2 geosequestration monitoring system for was installed at CO2CRC Otway Project site (Victoria, Australia) in early 2020. The system is composed of five deviated ~1600 m deep wells equipped with distributed acoustic sensing (DAS) acting as seismic receivers and nine seismic orbital vibrators (SOV) as seismic sources. DAS recording is performed continuously by three iDASv3 units. Each SOV operates for 2.5 h at a time, and hence all SOVs operating sequentially (during daytime only) produce in a single vintage every two days. Each vintage consists of 45 offset VSP transects covering predicted CO_2 plume migration paths over ~0.7 km^2 area. An automated data processing implemented on-site reduces data size from ~1.3 TB/day to ~500 MB/day with the results transmitted to the office daily.

The repeatability analysis based on pre-injection data (acquired from May to October 2020 before the injection start in December 2020) shows that variability of SOV performance is the main source of non-repeatability while borehole measurements are stable. An SOV waveform could reach NRMS value from 20 to 100 % within a few days. However, deconvolution of the seismograms with the waveform of the direct wave reduces the repeatability to within 10–15 % NRMS.

1. Introduction

Seismic methods are very useful for monitoring and verification programs for carbon capture and storage (CCS) projects in saline aquifers because the seismic properties of these reservoirs are often sensitive to the presence of supercritical CO_2 (Davis et al., 2019). In particular, time-lapse (TL) surface seismic – a series of repeated 3D seismic surveys has become a standard tool for delineation of a CO_2 plume (part of the subsurface occupied by the injected gas). A number of CO_2 projects around the world have reported clear TL anomalies associated with the injection of CO_2 Sleipner (Norway) (Chadwick et al., 2009), Aquistore (Canada) (Roach and White, 2018), Ketzin (Germany) (Lüth et al., 2017), Otway (Australia) (Pevzner et al., 2017a) and Decatur (USA) (Bauer et al., 2019). Analysis of these TL anomalies pursues two main objectives (Wildenborg et al., 2014):

Verify CO_2 plume containment: the absence of any leakages from the allocated part of the reservoir (Jenkins, 2020);
Prove CO_2 plume conformance: predictions of existing reservoir models agree with the observe migration of the injected gas (Oldenburg, 2018).

Fulfilment of both monitoring objectives may require frequent snapshots of the subsurface, which is often unfeasible for conventional TL seismic - an expensive technology in terms of both financial costs and the time lag between data acquisition and processing. Another complication may arise due to limited land access to storage sites because many

* Corresponding author at: Department of Exploration Geophysics, 26 Dick Perry Ave, Kensington, Western Australia, 6151, Australia.
E-mail address: roman.isaenkov@postgrad.curtin.edu.au (R. Isaenkov).

https://doi.org/10.1016/j.ijggc.2021.103317
Received 14 December 2020; Received in revised form 15 March 2021; Accepted 22 March 2021

CCS projects are likely to be located close to an industrial source of the captured gas. Hence, time intervals between the TL surveys are typically on the order of years, which may be inadequate for containment monitoring. Between surveys, a site operator must rely on production data and a limited set of downhole measurements, such as pore pressure and temperature (Benson et al., 2004; Hannis, 2013). These non-seismic monitoring methods lack spatial coverage and resolution to detect a CO_2 leakage that may occur hundreds of meters away from a borehole. In addition, calibration of the reservoir models to sparse snapshots of plume evolution is poorly constrained, which may compromise the conformance fluid flow simulations (Arts et al., 2003).

One way to address these challenges is by continuous seismic monitoring using permanently installed seismic equipment (sources and receivers). Despite high upfront costs of the installation, continuous monitoring is economic, because the data acquisition and processing can be fully automated and performed remotely with minimal labour costs. In addition, permanent systems have low environmental and/or societal impact, which allows them to operate at almost any time. Pioneering technology in this field, SeisMovie® by CGGVeritas (CGG, 2002), can provide automated daily updates of a reservoir image using 49 permanent borehole source points and 1500 hydrophone points over an area of 1.5 km^2 (Lopez et al., 2015). More recent advancements in continuous seismic monitoring are associated with distributed acoustic sensing (DAS), a relatively new technology that allows measuring dynamic strain along a fibre-optic cable, thus transforming the cable into a dense array of seismic sensors (Hartog, 2017; Parker et al., 2014).

DAS uses optical fibre to measure axial strain or strain rate along with the fibre (Bakku, 2015). In essence, the optical fibre becomes a several kilometres line of seismic receivers with channel spacing up to first tens of centimetres. Compared to conventional geophones, DAS with a standard single-mode fibre (SMF) lack directional sensitivity and SNR ratio. However, development of engineered fibres (Shatalin et al., 2021) improves DAS sensitivity substantially making DAS data quality comparable to that of geophones (Correa et al., 2017).

In recent years DAS technology was utilised for monitoring of CO_2 storage using Vertical seismic profiling (VSP) (Otway (Pevzner et al., 2020b), Decatur (Couëslan et al., 2013), Aquistore (White, 2019)). These studies show the high potential of TL 2D and 3D VSP for storage monitoring. Compared to surface seismic setup, borehole-based receivers have much better coupling with the formation and are more stable, resulting in lower TL noise. On the other hand, the number of monitoring wells is limited by high drilling cost thus reducing possible image coverage.

Seismic orbital vibrator (SOV) is a permanent seismic source which excites seismic waves by rotation of eccentric weights by an AC induction motor. SOV is a source of P and S waves as rotations produce both vertically and horizontally polarized force (Correa et al., 2018; Daley and Cox, 2001). The emitted seismic energy increases as angular frequency squared due to spinning origin of the source; this results in unbalanced frequency content. Unlike a similar permanent source ACROSS (Nakatsukasa et al., 2017), SOV lacks phase control and thus requires synchronisation using a recording of the source signature by a nearby geophone (Freifeld et al., 2016).

This paper presents a DAS VSP based permanent seismic monitoring system with SOVs deployed for Stage 3 of the CO2CRC Otway Project (Victoria, Australia). Stage 3 focuses on testing and development of cost-effective approaches to containment monitoring for CO_2 storage projects (Jenkins et al., 2017), and hence continuous multi-well offset VSP has naturally become a key component of this project. To simulate a leakage, 15,000 tonnes of supercritical CO_2/CH_4 (80/20 by molar volume) mixture (referred to as CO_2 below) will be injected into a saline clastic aquifer at 1550 m. Then CO_2 is expected to quickly move up-dip and form a relatively narrow plume elongated along an impermeable fault (Bagheri et al., 2020). Such a rapidly evolving plume provides a good test for the capabilities of the multi-well offset VSP. Some of the key uncertainties for the monitoring were resolved at a previous phase of the Otway Project, Stage 2C, which featured a very similar injection into the same reservoir (Pevzner et al., 2020b). In particular, we know that CO_2 saturation will likely cause a significant reduction of the rock stiffness, which allows for a confident detection of a small amount of CO_2 at seismic resolution (Caspari et al., 2015; Glubokovskikh et al., 2020; Pevzner et al., 2017a). Furthermore, the seismic sources and DAS receivers deployed at the Otway site provided an excellent signal-to-noise ratio (SNR) in the field tests, thus enabling robust interpretation of the TL response in the offset VSP data (Correa et al., 2018; Egorov et al., 2018, 2017). Therefore, design of the seismic monitoring system for Stage 3 focused on three main objectives:

1 Maximising the value of information in the data, such as increased spatial coverage, reduced probability of false detection of CO_2 plume arrival, accurate seismic estimates of the plume parameters;
2 Automation of the data processing and acquisition;
3 Stability of the instrumentation and hardware, including computing facilities and data transfer infrastructure.

Installation of the monitoring system was completed in February 2019 (Bagheri et al., 2020), and includes nine sources permanently deployed on the surface and five ~1600 m deep wells instrumented with advanced DAS systems (Fig. 1).

The paper is organized as follows. We begin with a summary of the pre-Stage 3 field tests at the Otway site, which determined the monitoring system design. We then give a detailed description of the system and an automated data processing workflow along with the processing/storage hardware. This is followed by the analysis of the data quality, system stability and performance over the first ~130 days of pre-injection monitoring.

2. Summary of the seismic monitoring at the Otway site

As indicated in the introduction, the seismic monitoring program for Stage 3 (active phase from 2019) of the CO2CRC Otway Project is based on field trials conducted at the Otway site during Stage 2C injection experiment (2015–2018) designed to test the sensitivity limits for the detection of a small leakage by conventional surface TL seismic (Cook, 2014). To this end, 15,000 tonnes of supercritical CO_2/CH_4 (80/20) mixture were injected at very low pressure (~200 kPa) through a dedicated CRC2 well into the Lower Paaratte formation, a sandstone brine-saturated reservoir located at a depth of 1500 m (Dance, 2013). Stage 3 involves a similar injection of 15,000 tonnes of supercritical CO_2 into the same formation through the CRC3 well, which is 700 m east from CRC2.

Pevzner et al. (2020b) give a detailed summary of the seismic monitoring program for Stage 2C; here we just summarise the main monitoring techniques. The key component of the TL seismic was a permanently deployed geophone array, which was buried at 4 m depth below the surface. The surface seismic program consisted of six repeat 3D seismic surveys acquired with a 15 klbs vibroseis truck: a baseline and five monitors acquired during and after injection (Popik et al., 2020). Concurrently with the surface seismic, 3D VSP was acquired in CRC1 well with a ten-level geophone tool positioned ~900 m deep. At the completion of each surface seismic vintage, a set of five offset VSPs were acquired in CRC-1 well. The main findings of the Stage 2C that contributed to the design of the Stage 3 monitoring program are:

1 TL seismic was able to detect as little as 5,000 tons of supercritical CO_2 fluid and image subsequent plume changes (Glubokovskikh et al., 2016; Pevzner et al., 2017a; Popik et al., 2020). This means that the seismic properties of the Lower Paaratte formation reservoir are very sensitive to the presence of CO_2 in the pore space;
2 3D VSP shows a clear plume image that agrees with the surface TL seismic;

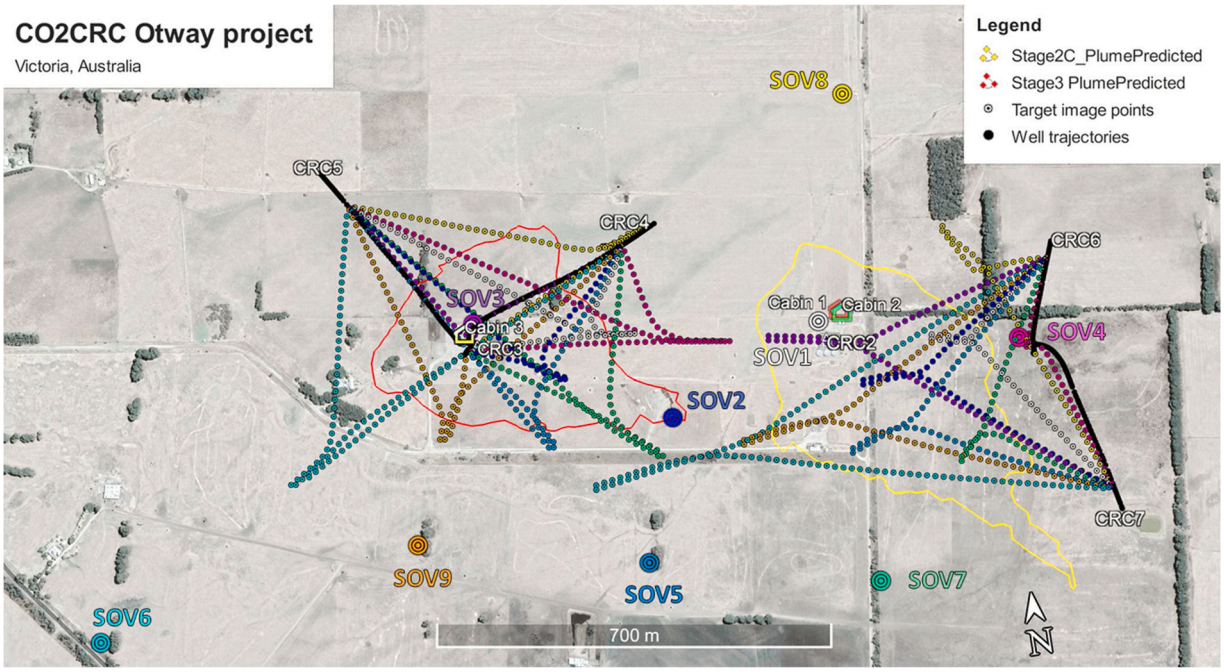

Fig. 1. Location of monitoring wells (CRC3-CRC7), SOVs and cabins on Otway site. Small circles are imaging location at the reservoir level (1500 m depth) where colour corresponds to the SOV number. Simulated plume contours for Stage 2C (yellow) and Stage 3 (red) plumes at the end of Stage 3 injection are given for minimum CO_2 saturation of 1% and minimum plume thickness of 4 m (Jenkins et al., 2018).

3 Offset VSP in CRC1 using a 3C geophone tool has a clear TL response. Egorov et al. (2017) obtained quantitative estimates of the plume properties (thickness, reduction of the compressional velocity) using full-waveform inversion (FWI);
4 Surface orbital vibrators (SOVs) were proven to be a reliable source of seismic signal with a repeatable signature and sufficient bandwidth. Weather effects on the near-surface conditions are the main source of the TL noise in the data (Yavuz et al., 2019).

In addition to the four field experiments listed above, a few tests were conducted after completion of CRC3 well, an injector for Stage 3, which focused on the performance of DAS receivers cemented behind the casing:

1 Correa et al. (2017) showed that for offset up to 1 km at the target interval, SNR of the DAS data are at least comparable to that of geophones;
2 Egorov et al. (2018) showed the feasibility of FWI for TL DAS data;
3 Offset VSP with the combination of SOV and DAS detected the injected CO_2 plume (Correa et al., 2018);

Besides the learnings related to the performance of seismic techniques, Stage 2C provided a refined reservoir model of the Lower Paaratte formation. History-matching of the TL images of the injection highlighted several geological features that control the CO_2 flow, such as sub-seismic faults and sandstone/mudstone transitions (Dance et al., 2019; Glubokovskikh et al., 2020). Also, the observed plume dynamics in Stage 2C constrained the range of dynamic parameters, such as relative permeability and CO_2 saturation threshold on the gas mobility.

3. Seismic monitoring system for Stage 3

The improved understanding of the Lower Paaratte formation and capabilities of the SOVs and DAS-based offset VSP underpinned the design of Stage 3 seismic monitoring system. The system aims to provide optimal coverage (number of seismic rays reflecting from a given area of the subsurface) over the CO_2 plume predicted by the pre-injection reservoir simulations (Bagheri et al., 2020).

3.1. Wells

Four deviated monitoring wells (CRC4-CRC7) were drilled and seven SOVs were installed on the site in January-February 2020 (Fig. 1) (Bagheri et al., 2020; Pevzner et al., 2020a). Well locations were chosen to optimise pressure and seismic monitoring and based on the predicted plume location. Five deviated wells are drilled from two pads to reduce the drilling cost and environmental footprint. All wells are drilled to a depth 100 m below the reservoir. CRC4 and CRC5 wellheads are located next to CRC3 in the north-western part of the site. CRC4 deviates to the north-east direction, CRC5 – to the north-west. CRC6 and CRC7 are located 1 km to the east from CRC3. CRC6 deviates to the north and CRC7 deviates to the south. To facilitate future quantitative interpretation of the DAS measurement, all new wells have sonic logs starting from the depth of 900 m to the bottom hole and zero-offset VSP.

Boreholes extend beyond the depth of the storage reservoir with a total true vertical depth of about 1600−1700 m. The well paths start deviating after 500−800 m depth and then reach maximum inclination angle of 20°. DAS directivity, which may be approximated as $\cos^2\Theta$, where Θ is the angle between the fibre and particle displacement in the incident wave (Bona et al., 2017; Correa et al., 2017; Kuvshinov, 2016). In the following, we detail the installation of the instrumentation and electronics.

3.2. DAS units and fibre installation

The fibre-optic sensors are interrogated by three recording units iDASv3 Carina (Silixa Ltd) (Shatalin et al., 2021):

- iDASv3 #1 → CRC4 and CRC-3 wells;
- iDASv3 #2 → CRC7 and CRC-6 wells;
- iDASv3 #3 → CRC5 well and a Helically Wound Cable (HWC) buried in a shallow trench about 1000 m long between SOV3 and SOV4 (HWC data are not analysed in this study).

Compared to most DAS systems, iDASv3 Carina™ system uses a specially engineered fibre (called Constellation™) with regularly spaced high optical reflectivity markers (Shatalin et al., 2021), which increases the sensitivity of the receiver and reduces system noise substantially.

Such a design, one DAS unit per two receiver lines, is a compromise between a relatively high cost of a DAS unit, and the maximum length of the connected fibre to provide sufficient SNR. The longer the fibre the fewer laser pulses may be sent per second and the higher attenuation losses are within the fibre (Pevzner et al., 2018). DAS units use 10 m gauge length, 1 ms sampling rate, 16 kHz pulse repetition frequency and 4 m pulse length. One DAS unit is connected to about 5-6 km of fibre in total. In iDASv3 Carina system, the reflectivity markers are 5 m apart in the fibre, hence the minimum interference between the backscattered signals is achieved for 10 m gauge length and 4 m pulse width. Along with the sampling interval of 1 ms and 16 kHz pulse repetition frequency, these parameters of the DAS systems provide excellent SNR as was shown in the field tests by (Pevzner et al., 2018).

Fig. 2 outlines the recording system for iDASv3 #2. First, a piece of single-mode fibre (SMF) buried in a trench connects to the DAS unit and the SMF cemented behind the casing of CRC7. Then SMF goes from CRC7 wellhead to the bottom of the hole (BH) where it is spliced to the constellation fibre (CF) (SMF and CF are physically in the same cable). Then CF reaches the wellhead of CRC7 where it is linked through the piece of trenched SMF to the CF at the wellhead of CRC6. The CF goes to BH, where it is spliced to the SMF and goes from BH to the wellhead of CRC6. The end of the fibre is connected to the attenuator to reduce the fibre's edge effects. The surface SMF is deployed in a trench to reduce the noise level and secure the fibre from potential damage.

3.3. SOVs

Seismic orbital vibrator (SOV) is deployed on a concrete plate. A pilot SOV dataset at Otway was acquired in March 2016 and showed good repeatability and frequency content of up to 80 Hz (Dou et al., 2017). These results showed the feasibility of using SOV as a permanent source for monitoring purpose. Yet this source has two shortcomings. The SOV lacks phase control of the rotating eccentric mass, which results in decreased repeatability of the source signature. Moreover, the magnitude of the signal is proportional to centrifugal acceleration and thus increases as frequency squared resulting in lack of energy at low frequencies. However, source phase may be compensated during processing using sweep recorded by 3-component geophone buried 3 m below the SOV. Stacking of sweeps improves SNR in general which is most important at low frequencies.

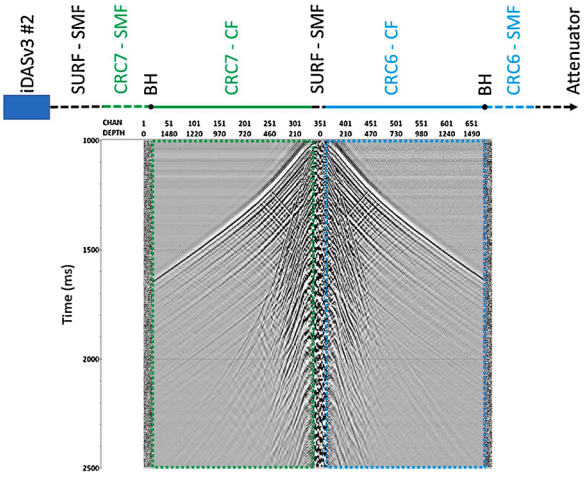

Fig. 2. DAS fibre connectivity in CRC7 and CRC6 wells (Top) and corresponding shot gather acquired by SOV4 (bottom). iDASv3 is designed to operate an engineered fibre and produces lower data quality in SMF. Start of recording time is 1000 ms after the start of SOV rotation.

To ensure a broad frequency band of the source signal, each SOV source consists of two motors of different sizes: a small motor (5 ton-force at 120 Hz; 70–105 Hz bandwidth) and a large motor (10 ton-force at 80 Hz, 8 Hz–80 Hz bandwidth). SOV3-SOV9 can operate both motors simultaneously while SOV1 and SOV2 have only one motor each. The SOVs are set to run 22 clockwise (CW) and 22 counterclockwise (CCW) sweeps of 150 s duration, which are recorded during a 2.5 h operation time for each SOV. To minimise the acoustic noise impact on the local community, the sources operate only in the daytime. It requires two days in total to run all SOVs.

CW and CCW rotations generate P waves of the same polarity and S waves of opposite polarities. Thus, the summation of CW and CCW is expected to enhance P waves and attenuate S waves while the subtraction of CW and CCW has an opposite effect (Dou et al., 2016). The CW and CCW summation is useful because we are primarily interested in reflected P waves. However, preliminary tests show that CW and CCW sweeps have different waveforms and thus a simple summation/difference provides a little gain in the data quality and more sophisticated processing procedures are required.

Given the trajectories of the wells, SOV locations are chosen to increase the seismic coverage over the predicted CO_2 plume. To ensure sufficient coverage and plume detectability, TL seismic response for given SOV locations (shown in Fig. 1) was simulated using finite-difference modelling. For simplicity, one may assume that reflection points illuminate the first half of the transect formed by a well-SOV pair, 45 transects in total. Furthermore, each of the deviated wells is aligned with an SOV to form a vertical 2D section: NE-SW (CRC3, CRC4 and SOV8, SOV3, SOV6), NW-SE (CRC5, CRC4 and SOV3, SOV5), S-N (CRC7 and SOV4, SOV8) and N–S (CRC6 and SOV3, SOV7) (Fig. 1). A 2D offset VSP geometry enables the application of 2D FWI (Egorov et al., 2018), which would be much more challenging in 3D with a sparse source coverage.

Note that in the offset VSP geometry, each reflection point is created by one source and one receiver, and thus fold is one for nearly all image points. An exception could be areas in the vicinity of vertical wells. Thus, the coverage is essentially represented by the density of image points at the reservoir level (rather than fold) given in Fig. 1.

3.4. Hardware infrastructure

Continuous monitoring using DAS generates an enormous amount of data that could not be transferred to a remote processing centre. To enable real-time processing, extensive computing infrastructure is deployed at the site. The hardware for the continuous monitoring system is installed in three seismic cabins (Fig. 1, Fig. 4). The data collection/processing system includes one main processing server (50 terabytes storage), five pre-processing servers, two backup/archive servers, two storage servers (80 terabytes storage each), and two 40-slots tape libraries (480 terabytes each). Each cabin has a 25 Gb network switch to accommodate fast data transmission between the hardware components.

Cabin 1 is the only cabin that has Internet access, including LTE (Long-Term Evolution standard for wireless connection) and NBN (Australian National Broadband Network) links. These internet links are used to connect to one of the two gateway machines (Gate1 and Gate2) for remote access to all servers and enable data transfer from and to the facility. Cabin 1 houses a stratum-1 NTP (Network Time Protocol) time server, which guarantees the time synchronisation. In addition to these, Cabin 1 has a weather station and distributed temperature sensing (DTS) unit.

Cabin 2 has the main processing server, two pre-processing servers, one archive server, one tape library and a storage server. It communicates with Cabin 1 via a 1 Gb fibreoptic link. SOV sweeps recorded by 3C geophones are transferred to the storage server in Cabin 2. The iDASv3 #2 unit is located in Cabin 2 and continuously acquires data from CRC6

and CRC7 wells (Fig. 4). Data form the unit are pre-processed by a dedicated server and the raw records are archived on tapes by two storage libraries in Cabins 2 and 3.

Cabin 3 has two DAS units, iDASv3 #1 and iDASv3 #3, three pre-processing servers, one archive server, one tape library and a storage server. Cabin 3 communicates with Cabin 2 via 50 Gb link (see Fig. 3 diagram for fibre types). Data from each unit are pre-processed by a dedicated server and raw records from iDASv3 #1 and iDASv3 #3 are archived on tapes by two storage libraries in Cabins 2 and 3.

4. Automated data processing

The DAS data is recorded continuously for passive monitoring. Then, the SOV records are selected from the continuous recording based on precise GPS time. The processing implements a set of standard offset VSP procedures. Optimal processing parameters are based on the first vintage acquired in May 2020. The parameters are hand-tuned for each SOV-well pair. Then the optimal parameters are applied repeatedly in the automated real-time data analysis (Yavuz et al., 2020).

4.1. Processing flow

Table 1 outlines the main processing steps. First, we decimate the data by resampling it from 1 to 2 ms and stacking channels into 5 m bins. That decimation is valid as iDASv3 is designed to sample wavefield at 5 m intervals and we expect no frequencies above 250 Hz. Thus, neither decimation nor binning affects the information content but reduces data size by an order of magnitude.

The decimation and binning are followed by deconvolution of the record with the SOV source sweep recorded by 3C geophones. As discussed earlier, the power spectrum is strongly biased towards high frequencies. Thus correlation, commonly used in Vibroseis seismic, will make SOV spectrum even more unbalanced. Instead, we use deconvolution with the recorded sweep, which makes the energy more evenly distributed across the frequency bandwidth (Daley and Cox, 2001). Next, all repeated CW and CCW sweep seismograms are stacked separately. At this point, the amount of data drops to 500 MB/day compared to the initial 100 TB/day.

Unlike the position of geophones, the exact location of each DAS receiver is not known precisely. Indeed, DAS measurement is spatially distributed (average strain rate over given gauge length) and its location along the fibre is measured by the laser pulse travel time and speed of light in the fibre. The latter is not known precisely. A 1% error in the speed of light results in the 10 m error in distance estimation at 1000 m. 6000 m of fibre can result in an error of about 60 m at the end of the fibre.

Fortunately, there are at least two locations on the DAS cable which are known exactly: BH and the wellhead. The fibre changes from Constellation to single-mode fibres at BH, resulting in a significant SNR change (Fig. 2). We locate the wellhead as the beginning of the region where upgoing waves reflect from the free surface and create downgoing waves. When both of these locations are identified on DAS data, we interpolate the geometry in-between based on the well deviation survey. Then, we remove all channels which are outside the well or contaminated by noise.

Signature deconvolution is an essential step that compensates for the variations of the source signature over time. We call it 'designature' to distinguish it from sweep deconvolution. Designature is done in two steps. First, we estimate the `source' wavelet for each well-SOV pair and rotation by stacking the direct wave signal in ~700−1500 m depth interval (specified for each pair). The designature is followed by a band-pass filter to shape the resulting wavelet and remove the noise outside the useful bandwidth.

At the next step, a set of FK filters separates the wavefield to isolate and retain only primary PP reflections (which are later used for imaging). For far offsets (e.g. SOV6 and any well) the separation is challenging because P and S travel-times are almost flat and the FK filter is ineffective. Moreover, at large offsets (e.g., target reflections in CRC5-SOV7 and -SOV5), the very detection of PP waves becomes challenging as these waves arrive nearly normal to the fibre and hence DAS receivers are almost insensitive to them. However, PS waves are still clearly visible for such offsets and may be very useful for imaging.

The final step is 2D time migration. The migration 1D velocity model is built based on the zero-offset VSP first break travel times. Then, we use the anisotropic NMO equation (Alkhalifah and Tsvankin, 1995) to approximate the travel time field and straight rays for estimation of the offsets and angles. Then, the seismic image is formed by stacking the seismic amplitudes along the isochrones for each image point in a narrow 3° aperture. Amplitude scaling prior to stacking is based on Dillon (1990) VSP Kirchhoff migration algorithm. Since most of the wells are deviated, imaging points form a curved surface for most of the VSP-pairs (Fig. 5d). As an example, Fig. 4 shows the results of the key processing

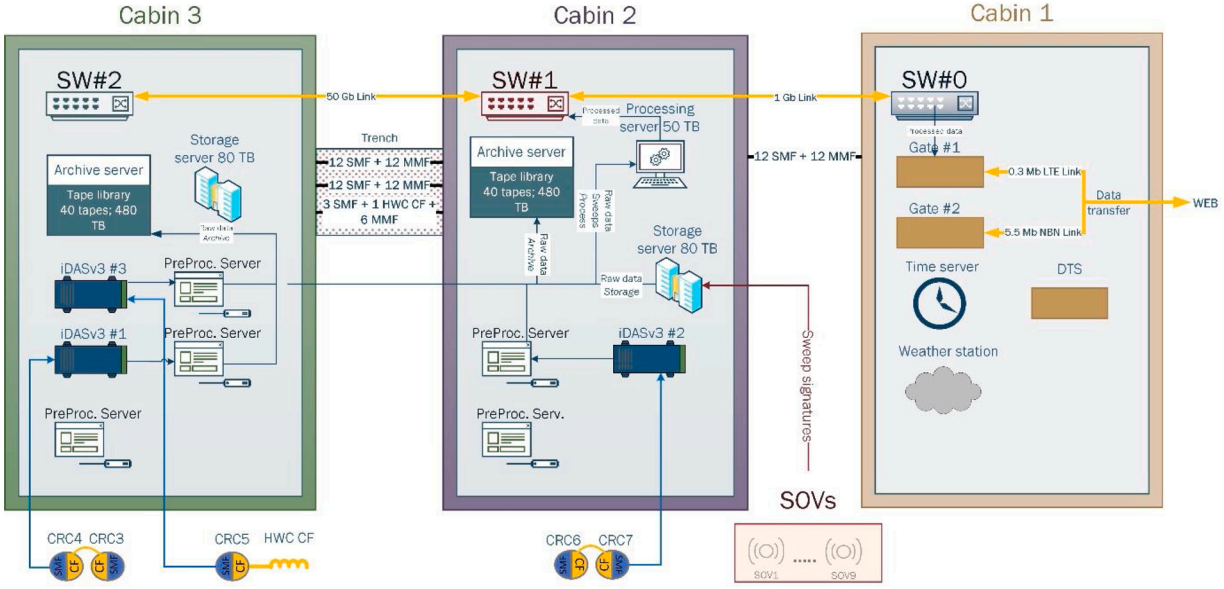

Fig. 3. Hardware setup of the automated continuous monitoring system at the Otway research site. SMF – single-mode fibre, CF – Constellation fibre, HWC – helically wound cable.

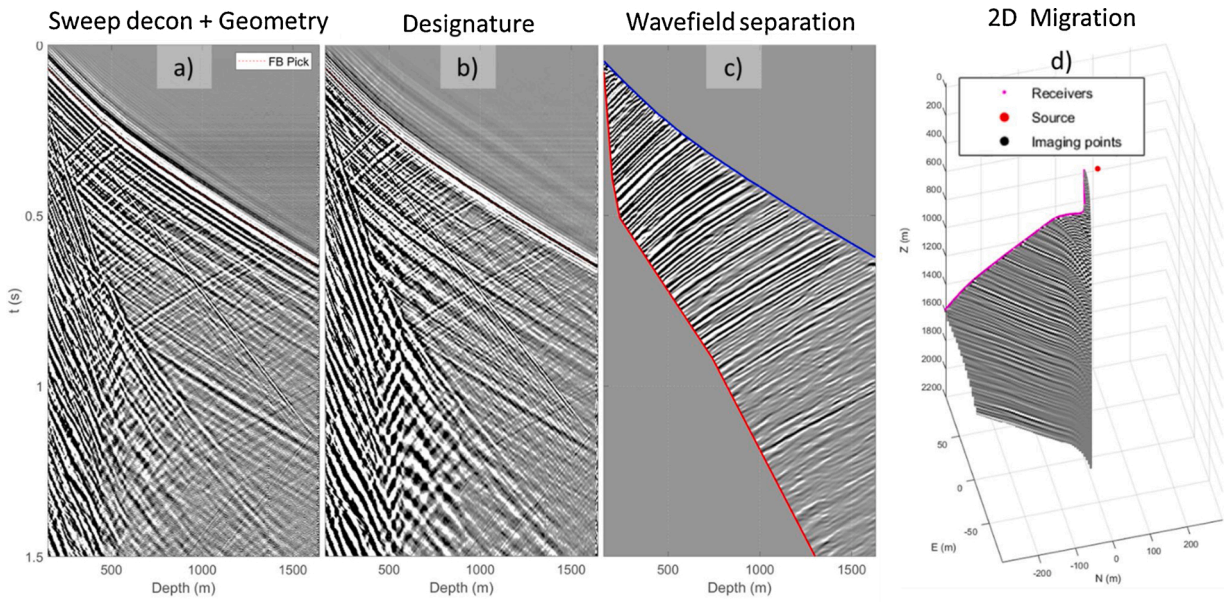

Fig. 4. Seismograms after key processing steps for CRC7-SOV4 pair with the optimal parameters: sweep deconvolution and geometry assignment (a), designature (b), wavefield separation and muting (c) and 2D Migration (d). Refer to Table 1 for more details.

Table 1
2D DAS-SOV VSP data processing flow.

Procedure	Details
Data input	Not correlated data for each well-SOV pair
Data decimation	Resampling the DAS data from 1 ms to 2 ms and binning channels from 1 m to 5 m
Sweep Deconvolution	Deconvolution with the sweep recorded by the SOV geophone
Vertical Stacking	Stacking the seismograms for the sequential SOV sweeps
Geometry	Assigning receiver (DAS) and source (SOV) geometry
Wavelet estimation	Wavelet estimation from the direct wave
DESignature	Deconvolution with the estimated wavelet
Bandpass filter	Application of a bandpass filter (specific for each SOV-well pair)
Wavefield separation	Application of FK filters to remove downgoing S- and upgoing S- and PS-waves (specific for each SOV-well pair)
Amplitude correction	Compensation for the spherical divergence
Migration	Kirchhoff migration in time domain, central dip = 0, image grid step dx =5 m, dz =1 m. 1D isotropic velocity model from zero-offset VSP.

steps for the SOV4 - CRC7 pair.

4.2. Data flow

As discussed above, there are many steps between initial DAS records and the final migrated images. After 1.5 days from the first commencement of rotation of the first SOV, the system produces a QC report with the images. At this point, the original data size is reduced from about 100 TB to 500 MB. During these steps, data is sent from the DAS units to the processing and storage servers with the final results being sent daily to the office at Curtin University (Perth, Australia). In this section, we describe the flow of the data on the site and the time it takes to acquire, process and archive the data.

Fig. 5 details the data flow from the DAS units to the office along with the corresponding data size and processing time at each step. Running four or five SOVs takes about 10–12.5 hours each day. The first SOV starts rotating at about 10 pm UTC and the last SOV finishes at about 11 a.m. UTC the next day. The passive data is recorded for another 13 h until midnight UTC.

The raw DAS data is backed up on two tape libraries for another 8 h. The data decimation begins when the back-up finishes at one of the tape libraries: one preprocessing server per DAS unit resamples the data for 1.5 h. Then, the decimated seismic data is moved to the storage server and processing begins. Sweep deconvolution – the longest step - takes about 3 h. During the next 20 min, the data is processed from the initial gathers to migrated images. All controlling scripts are implemented in MATLAB and are executing sequentially all the processing and archiving the recorded data.

Continuous recording of three DAS units produces around 200 TB of data per vintage in an internal SIlixa ltd format. Fig. 6 illustrates the data size reduction in the automatic processing flow. Over the entire course of the flow, data volumes are reduced by a factor of around $3 \cdot 10^6$. First, data is down-sampled at the interrogation unit (IU) from 16 to 1 kHz sampling frequency and from 0.25 to 1 m spatial sampling. Then, during software decimation, data is resampled further to 5 m channel spacing and 2 ms in time, reducing the data size by one more order of magnitude. Next, the sweep deconvolution converts the effective seismic record length from 150 s (duration of a sweep plus listening time) to 4 s, which results in a reduction of the size to 20 GB per vintage. Then, stacking of all the CW and CCW sweeps within the same vintage and SOV-well pair reduces the vintage size further to about 1 GB, which may be transmitted through the Internet. At this point, the stacked datasets are uploaded to the cloud storage and sent to the Perth office for time-lapse analysis and additional archiving. Then, the data size is reduced by a factor of two after geometry assignment, as some auxiliary and noisy channels are removed. Other processing steps such as designature (signature deconvolution) and wave fields separation do not reduce data size. Finally, 2D Kirchhoff provides an image of only 67 MB per vintage.

5. Discussion of pre-injection monitoring results

From the first vintage acquired at the end of May 2020 to the end of October 2020, the deployed monitoring system accumulated more than 130 days of data. During this period, the seismic properties of the injection interval could be affected only by a slow evolution of the Stage 2C CO_2 plume. This is expected to have a negligible effect on the seismic properties of the target interval as it is 700 m west from the previous injector while the plume is expected to migrate in the SE direction. Hence, we consider any time-lapse discrepancy between the pre-injection monitoring vintages as a time-lapse noise. Analysis of this

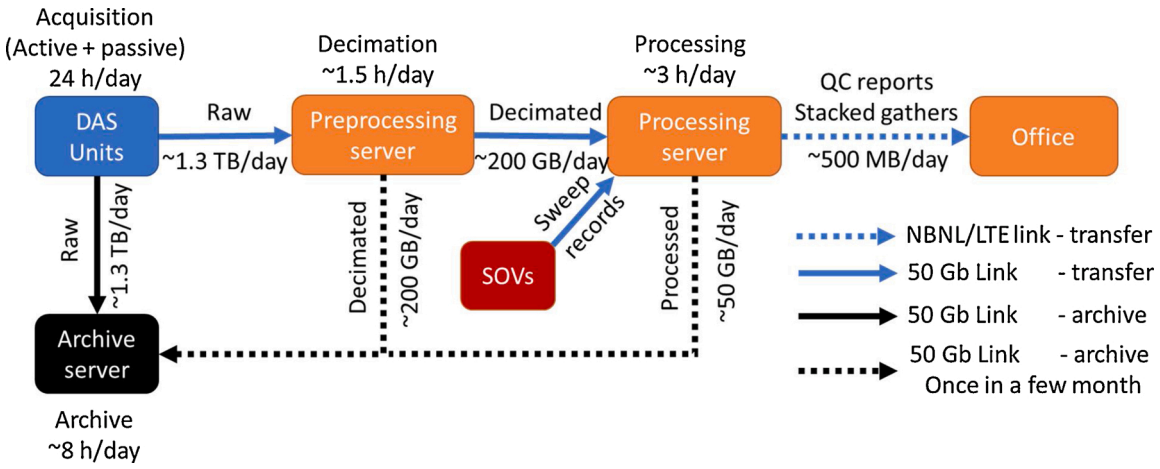

Fig. 5. Simplified data flow diagram. Data is recorded by DAS Units continuously. Once per 24 h it is backed up on two archive servers. When archiving is finished, data is decimated on the preprocessing server and processed on the processing server. Once a day QC reports and stacked gathers are sent to the office. Arrow labels indicate data flow direction and approximate data size. Approximate timing for each procedure is also given.

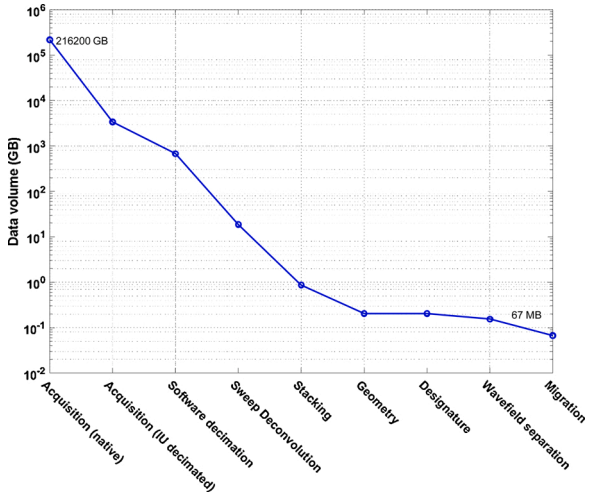

Fig. 6. Data volume reduction after each processing step (given in Table 1) in the automatic processing flow of continuously acquired data at the Otway research site. At the end of processing, the data volume is reduced from 216 TB to 67 MB. This illustrates the importance of on-site processing as transferring even 20 GB per 2 days (after sweep deconvolution) may be challenging.

noise provides a means to estimate three main factors that control the repeatability of the seismic signal and the detectability of the TL signal from the future Stage 3 injection: stability of the instrumentation, weather impact on the near-surface conditions and ambient noise.

5.1. Problems during acquisition

Permanent deployment puts extremely high weight on the stability of the instrumentation because a system break-down during rapid time-lapse changes would compromise continuous monitoring. During the trial period (May-October 2020) the Stage 3 monitoring system had seven incidents that resulted in a complete or partial loss of the monitoring vintages. Three categories of problems arose during the acquisition of 66 vintages (132 days): power outages, DAS Unit failures and SOV failures (Table 2). Corresponding intervals of missing data are clearly visible a TL SNR map (Fig. 7).

There were two full stoppages due to power outages. The first one was associated with construction works at the site and resulted in a loss of three vintages. The second power outage was due to a limited power supply at the site. While these incidents caused significant disruption to the Stage 3 system, electrical security may be less of an issue in a commercial project, where power supply for the boreholes/pumps is likely to be autonomous.

Table 2
Summary of technical incidents during 132 days of acquisition.

Event #	Vintages lost	Affected well(s)	Affected SOV(s)	Description
1	2.5	All	All	Power outage
2	17	CRC5	–	DAS Unit #3 failure
3	1	CRC3, CRC4	–	DAS Unit #1 failure
4	10	–	SOV6	SOV electronics damaged by ants
5	2	–	SOV5	Not operational
6	1	–	SOV1, SOV8	Electronics damaged by ants
7	1	–	SOV2	SOV radio connection is lost

Not all SOV s are equally critical for leakage monitoring, as some of the sources contribute to the plume image accuracy rather than its detection. SOV1 and SOV2 improve coverage (Fig. 1). Conversely, SOV6 illuminates the south-western part of the injection. That is why SOV6 failure over a period of ten vintages due to an infestation of the electronics by ants was of major concern.

Reliability of the DAS units is also of critical importance. Failure of one DAS unit leads to the loss of 20–40 % of the data. iDASv3 #3 (CRC5) covers the north-western part of the injection, iDASv3 #1 (CRC3, CRC4) – the central area of injection zone and iDASv3 #2 (CRC6, CRC7) the eastern area of the site. During and immediately after injection, the central area covered by CRC3, CRC4 and CRC5 is most critical.

Apart from these incidents, all SOV-well pairs show stable SNR with a maximum confidence interval of about ± 6 dB around the median value (Fig. 7, top graph) of about 30 dB. However, not all Well-SOV pairs have similar data quality. Generally, the SNR depends on the source-receiver offset: the closer the source the stronger is the signal, while the noise level remains almost constant. This explains why the most distant SOV (SOV6) has the lowest SNR (Fig. 7) resulting in low repeatability (Fig. 9).

The SNR map is a useful tool to examine the data quality. A change in SNR may indicate a deterioration of a piece of equipment or some irregular condition at the site. For example, failure of iDASv3 #3 was preceded by a gradual decrease of SNR by 10 dB in CRC5.

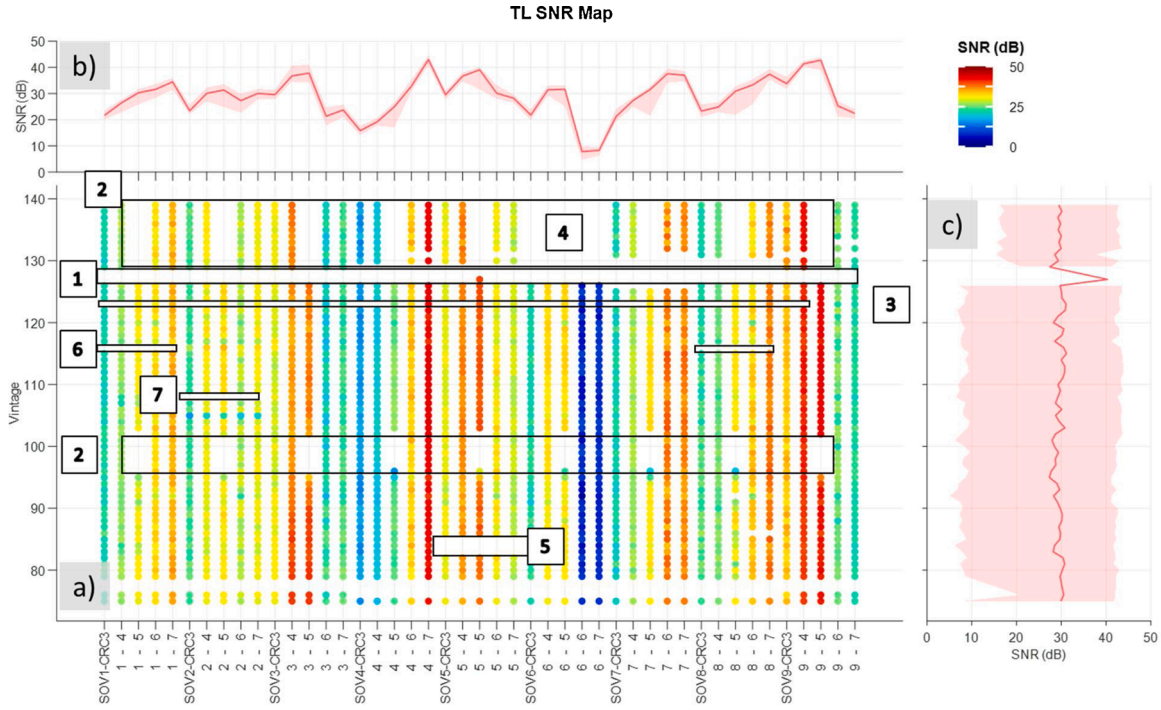

Fig. 7. TL SNR distribution after designature for each Well-SOV pair, CW rotation. Colour of each dot on the map (a) represents SNR for a given vintage number and Well-SOV pair. The graphs (b and c) represent median SNR (red line) and 95 % confidence interval (transparent red area) grouped by pairs (b) and vintages (c). Numbers in boxes are events listed in Table 2. One vintage corresponds to the two-day interval. RMS of the noise is estimated in a 400 ms window above first breaks; RMS of the signal is estimated in 150 ms window around first breaks in 900-1300 m depth interval.

5.2. Repeatability

When a monitoring array operates normally the non-repeatability of the seismograms is due to the following main reasons:

- Source: weather effect on SOV and/or the geophone recording of the sweep signal; SOV mechanical deterioration;
- Receivers: borehole condition, injection noise, temperature effects on DAS;
- Variability of coherent noise – each wavefield component other than PP reflections - caused by the variations of the near-surface conditions.

Sweep deconvolution compensates for variability in the SOV parameters. Unfortunately, both SOV and sweep recording geophone are affected by near-surface conditions. This leads to variation in the wavelet shape: Fig. 8a, c and e show the estimated wavelet and its power spectrum for the CRC7-SOV4 pair over about 130 days of acquisition. Although the wavelet shape remains similar, the change of the amplitude level is significant: it decreases by a factor ~3.5 first and then gradually returns to the initial level. Since SNR is stable for all records, the source energy should be similar for all vintages, and hence the variations are likely due to coupling of the SOV geophone to the ground (Fig. 7).

Such source fluctuations could compromise the data repeatability. However, the source signature can also be estimated from the direct wave arrival (average along the first breaks). Thus, the near-surface effect on the source signature or its recording by the geophone is compensated by the designature processing step. Fig. 8 shows drastic improvement in the repeatability after the designature.

Next, we access the repeatability of wavelets for all well-SOV pairs. We perform repeatability analysis by comparing baseline with one of the monitor vintages at a time. To quantify the repeatability of the wavelets we use normalised root mean square metric NRMS (Kragh and Christie, 2002):

$$NRMS = 2\frac{RMS\ (BS - VT)}{RMS(BS) + RMS(VT)} \quad (1)$$

where BS is the baseline signal, VT the vintage wavelet, and RMS is the root mean square of a time series.

The wavelet NRMS can be estimated before and after designature. If two wavelets are exactly the same NRMS equals 0, if both wavelets are random noise then NRMS equals ~ 1.4. The NRMS is sensitive to both amplitude variations and time shifts. Typical good repeatability NRMS is 0.1 – 0.3 (Johnston, 2013). In the Stage 2C of the Otway project, the CO_2 plume of as little as 5 ktonnes in the same Paaratte formation was detected with 4D seismic with an average NRMS of about 0.15 (Pevzner et al., 2017b). The data after sweep deconvolution has a clear trend towards the increase of NRMS (Fig. 9 a). NRMS after designature (Fig. 9b) becomes significantly lower with 0.02 NRMS for SOV2 and 0.2 NRMS SOV6 while average wavelet NRMS is about 0.1−0.15 NRMS. Such repeatability is only possible because of the availability of direct waves in the offset VSP seismograms.

When grouped by boreholes (Fig. 9c, d) we see that data have similar mean NRMS values: 0.4 NRMS before designature and 0.1 NRMS thereafter. This means that the main source of non-repeatability is SOV whereas the downhole DAS measurements are stable. However, the failure of a DAS is still the highest risk for monitoring. Another possible source of non-repeatability is a noise caused by the CO_2 injection itself and related site operations.

Fig. 10 gives the overall picture of the survey repeatability. Unlike previous figures, here NRMS is estimated as an average value for traces at 900−1300 m depth interval. This means that non-repeatable noise may not be cancelled out so effectively by averaging. Most of the pairs have stable NRMS of about 0.1 (see Fig. 7).

At last, dense time sampling of the vintages gives us a new way to analyse the data. We can plot vintages next to each other to get TL shot gather for each pair (Fig. 8 (a, b)). A time slice may help to indicate changes in a specific wavefield component. As the primary P wavefield

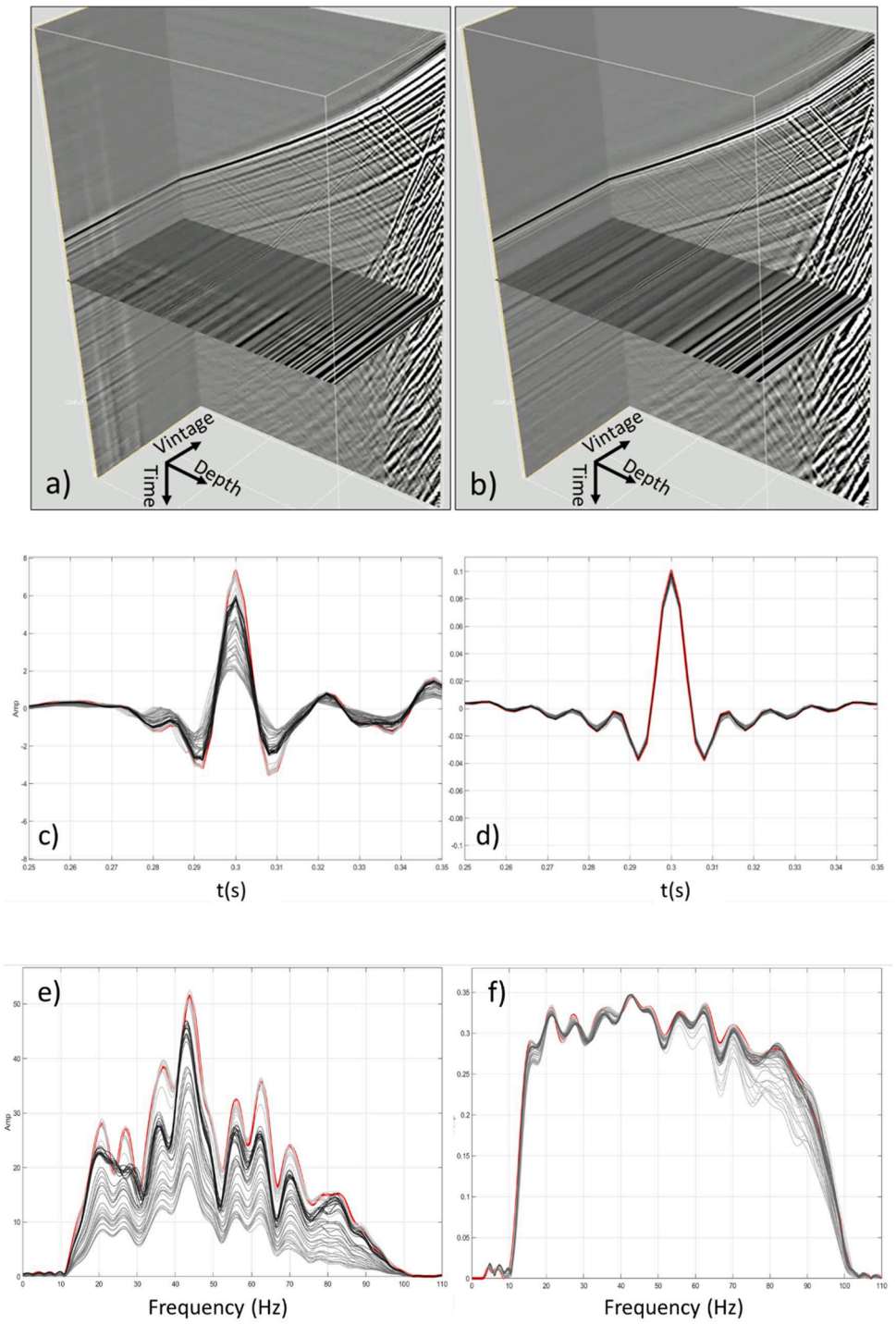

Fig. 8. Time-lapse data after sweep deconvolution (a, c, e) and designature (b, d, f) for CRC7-SOV4 pair: TL shot gathers (a, b) in time-depth-vintage coordinates; extracted wavelet (c, d) and its spectra (e, f). Red lines correspond to the first vintage while gradation of grey represents vintage number – the lighter the colour the older the vintage.

variations are compensated via designature, we can visually detect variations in non-primary P and S wave arrivals. Such an analysis helps trace sources of non-repeatability. Furthermore, having many vintages can improve repeatability even farther with predictive filtering.

6. Discussion

First 130 days of the recording provided encouraging results in terms of the data quality and operability of the data management system. However, the Stage 3 array provides only 45 offset VSP transects that cover ~0.7 km^2 area. Compared to SeisMovie®, our monitoring design has relatively sparse spatial coverage and different VSP transects usually have different amplitudes for the same reflection points, which complicates the quantitative interpretation of the data.

The key to excellent repeatability is the availability of the source signature from the direct wave in VSP seismograms: designature reduces NRMS down to about 0.1−0.15. The recorded data show significant variations in SOV signal amplitudes (e.g. SOV4). It is unclear if the cause was a deterioration of SOV performance or a change of their coupling due to weather changes, as the shot gathers depend both on the signal

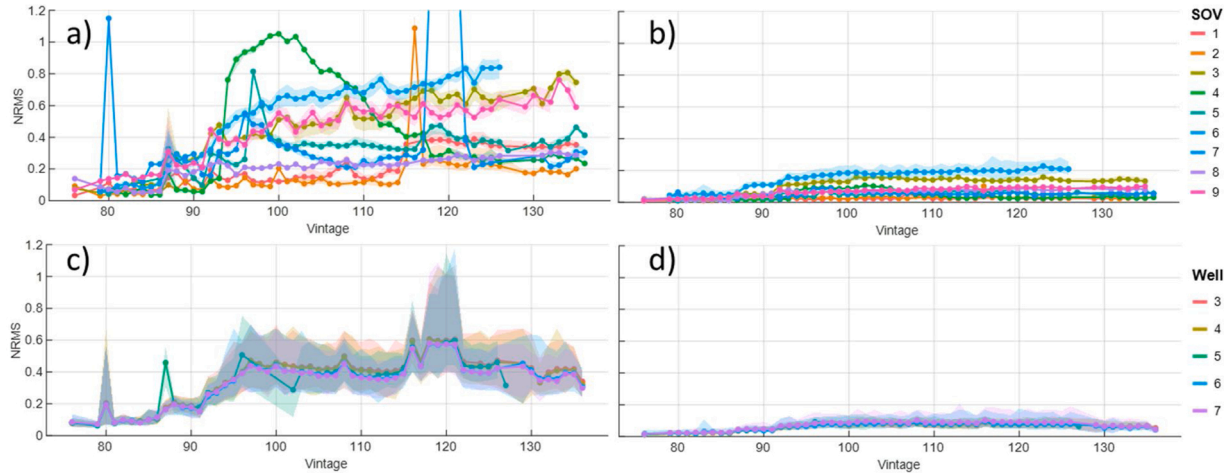

Fig. 9. NRMS of the estimated wavelets after sweep deconvolution (a, c) and designature (b, d). Data is grouped by SOVs (a, b) and by wells (c, d). Solid lines – mean NRMS, transparent area – standard error of the mean, colour code – SOV/Well number. The vintage number is a halved number of days from 1st January 2020. Note, that before designature non-repeatability grows steadily for most of the SOVs while NRMS for SOV4 is peaked from 0.15 to about 1 in only a few days. After designature, we still observe an increase in non-repeatability while the rate is quite small.

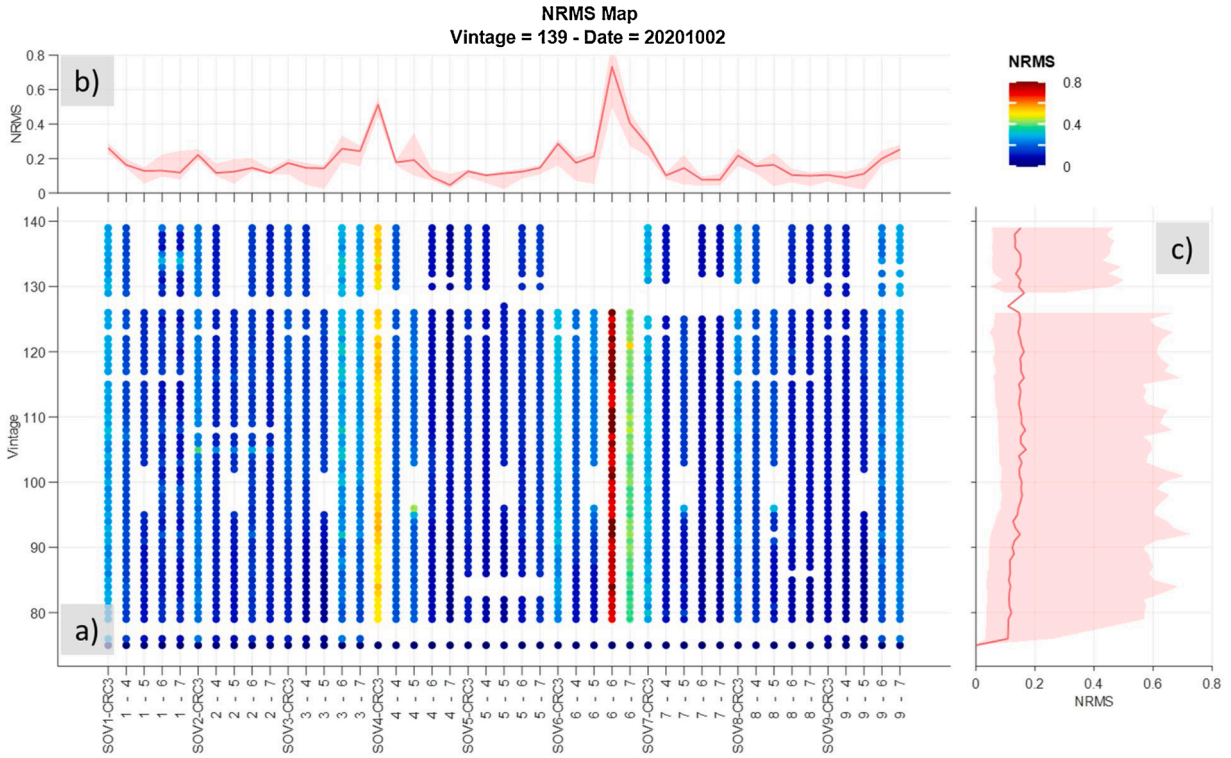

Fig. 10. Same as Fig. 7 but for NRMS instead of SNR. Note poor repeatability for SOV4-CRC3 and SOV6-CRC6,7. This is mainly due to large source-receiver offset. The average repeatability is about 0.1-0.15.

emitted by SOVs and on the medium where the pilot geophone is located. This could be further studied by analysing the effect of precipitation on DAS signals. This work is ongoing and beyond the scope of the present paper. To avoid weather effect on the geophone coupling it is preferable to deploy the pilot geophone below the water table (if possible).

In the trial period, the most significant contributor to the TL noise was malfunctioning of the instrumentation. To avoid possible data loss due to unit failure during injection and post-injection period, having a spare DAS unit on site is required. Another source of non-repeatability is near-surface variations. Even after compensation, these variations may affect surface-related multiples and S wave patterns which may interfere with primary P wave reflections. These effects will be analysed in a future study.

Our data quality analysis has focused on the direct wave. At the same time, the plume image will be formed by reflected waves, which have at least an order of magnitude lower intensity than the direct arrivals. Hence, the estimated high values of SNR levels and repeatability reported earlier is likely to be optimistic. Yet the repeatability can be improved substantially by stacking several sequential vintages.

Indeed, our analysis so far has mainly focused on the comparison of the same signals in two vintages at a time. Yet we have the entire history of the monitoring at our disposal and can implement a batch-processing of the sequential data (many vintages at once), such as Kalman filtering

(Evensen, 2009). This approach would reduce the probability of the false detection of the plume arrival and increase the confidence of the plume images. From that point of view, the pairwise-type of estimates of the repeatability may be underestimated.

Furthermore, the current workflow uses primary P-wave reflections only and ignores all other wavefields. Primary S-waves, converted waves and multiples have a high potential of improving coverage and, thus, detectability, and can be utilised by employing PS wave migration, full waveform inversion and seismic interferometry, which may help extract more value from the data.

We acquired the data for CW and CCW SOV rotation and processed them separately. Stacking and subtracting these two rotations have the potential to separate source generated P and S wavefields. This will help reduce the interference of wavefields and allow the use of S waves to improve the coverage.

7. Conclusions

The Proposed monitoring system allows acquisition of seismic vintages every two days in an automated manner. The permanent installation requires no human effort on-site and thus drastically reduces the monitoring cost. Such a system can coexist within industrial or farm area as it produces a tolerable level of noise and operates only within the allowed time schedule (in the daytime).

The survey design is based on previous studies at Otway, especially, Stage 2C. The choice of VSP geometry has three advantages over surface seismic: VSP does not interfere with the infrastructure, the receivers are not affected by the weather conditions and the source wavelet can be directly estimated from VSP data.

The permanent installation of equipment (DAS in wells and SOVs on the surface) allows setting a single processing flow for all vintages, which can be run autonomously without manual input. Results of QC and processing reports may be sent daily to the operator in the office.

Unlike DAS receivers installed in boreholes, SOVs are cemented at the surface and thus the source signature is affected by local near-surface variations. Such variations can alter not only the SOV signature but also 3C geophone employed to record sweep. Such signature variations may affect the repeatability of TL survey. Yet, borehole measurements make it possible to estimate SOV signature and remove variations from the data via deconvolution. Deconvolution corrects not only the wave shape but also amplitudes and time shifts. The average repeatability of processed data for the 130 days period is about 0.1−0.15 NRMS measured around the direct wave.

The short turnaround (2 days) monitor survey gives an opportunity to acquire about 180 vintages per year. Thus, each DAS-SOV dataset may be represented as a 3D volume in three coordinates: receiver location, travel time, vintage date. Thus, we can analyse seismic dataset as a time series and apply some advanced data assimilations techniques. Having seismic monitoring data almost daily may inform reservoir management decisions leading to a better understanding of the reservoir history and more effective CO_2 storage.

Author statement

Roman Isaenkov: Software, Formal analysis, Data Curation, Writing - Original Draft, Writing - Review & Editing, Visualization. **Roman Pevzner:** Conceptualization, Methodology, Software, Formal analysis, Investigation, Resources, Data Curation, Supervision, Project administration. **Stanislav Glubokovskikh:** Conceptualization, Methodology, Writing - Original Draft. **Sinem Yavuz:** Methodology, Formal analysis, Data Curation. **Alexey Yurikov:** Methodology, Formal analysis. **Konstantin Tertyshnikov:** Conceptualization, Methodology, Formal analysis. **Boris Gurevich:** Conceptualization, Supervision, Writing - Original Draft, Writing - Review & Editing. **Julia Correa:** Software, Formal analysis, Investigation, Resources. **Todd Wood:** Software, Resources. **Barry Freifeld:** Conceptualization, Resources, Supervision **Michael Mondanos:** Methodology, Resources. **Stoyan Nikolov:** Investigation. **Paul Barraclough:** Validation, Resources, Supervision

Declaration of Competing Interest

The authors report no declarations of interest.

Acknowledgements

The Otway Project received CO2CRC Ltd funding through its industry members and research partners, the Australian Government under the CCS Flagships Programme, the Victorian State Government and the Global CCS Institute. The authors wish to acknowledge the financial assistance provided through Australian National Low Emissions Coal Research and Development (ANLEC R&D). ANLEC R&D is supported by COAL21 Ltd and the Australian Government through the Clean Energy Initiative. Funding for LBNL was provided through the Carbon Storage Program, U.S. DOE, Assistant Secretary for Fossil Energy, Office of Clean Coal and Carbon Management through the NETL, under contract No. DE-AC02- 05CH11231.

References

Alkhalifah, T.A., Tsvankin, I., 1995. Velocity analysis for transversely isotropic media. Geophysics 60, 1550–1566.
Arts, R., Eiken, O., Chadwick, A., Zweigel, P., Van der Meer, L., Zinszner, B., 2003. Monitoring of CO_2 injected at Sleipner using time lapse seismic data. Greenhouse Gas Control Technologies-6th International Conference 347–352.
Bagheri, M., Pevzner, R., Jenkins, C., Raab, M., Barraclough, P., Watson, M., Dance, T., 2020. Technical de-risking of a demonstration CCUS project for final investment decision in Australia. Appea J. 60, 282–295.
Bakku, S.K., 2015. Fracture Characterization From Seismic Measurements in a Borehole. Massachusetts Institute of Technology.
Bauer, R.A., Will, R., Greenberg S, E., Whittaker, S.G., 2019. Illinois Basin–Decatur project. In: Wilson, M., Landrø, M., Davis, T.L. (Eds.), Geophysics and Geosequestration. Cambridge University Press, Cambridge, pp. 339–370.
Benson, S., Hoversten, M., Gasperikova, E., 2004. Overview of Monitoring Techniques and Protocols for Geologic Storage Projects. IEA Greenhouse Gas R & D Programme.
Bona, A., Dean, T., Correa, J., Pevzner, R., Tertyshnikov, K., Van Zaanen, L., 2017. Amplitude and phase response of DAS receivers. In: 79th EAGE Conference and Exhibition 2017. EAGE, Paris, France.
Caspari, E., Pevzner, R., Gurevich, B., Dance, T., Ennis-King, J., Cinar, Y., Lebedev, M., 2015. Feasibility of CO2 plume detection using 4D seismic: CO2CRC Otway Project case study — part 1: rock-physics modeling. Geophysics 80, B95–B104.
CGG, Gd.F., Institut Francais de Petrole, 2002. SeisMovie Aims to Be a Blockbuster for 4D Seismic Reservoir Monitoring. First Break, p. 20.
Chadwick, R.A., Noy, D., Arts, R., Eiken, O., 2009. Latest time-lapse seismic data from Sleipner yield new insights into CO2 plume development. Energy Procedia 1, 2103–2110.
Cook, P., 2014. Geologically Storing Carbon: Learning From the Otway Project Experience. CSIRO Publishing.
Correa, J., Egorov, A., Tertyshnikov, K., Bona, A., Pevzner, R., Dean, T., Freifeld, B., Marshall, S., 2017. Analysis of signal to noise and directivity characteristics of DAS VSP at near and far offsets — a CO2CRC Otway Project data example. Lead. Edge 36, 994a991–994a997.
Correa, J., Tertyshnikov, K., Wood, T., Yavuz, S., Freifeld, B., Pevzner, R., 2018. Time-lapse VSP with permanent seismic sources and distributed acoustic sensors: CO2CRC stage 3 equipment trials. 14th Greenhouse Gas Control Technologies Conference Melbourne 21–26.
Couëslan, M.L., Ali, S., Campbell, A., Nutt, W.L., Leaney, W.S., Finley, R.J., Greenberg, S. E., 2013. Monitoring CO_2 injection for carbon capture and storage using time-lapse 3D VSPs. Lead. Edge. 32 (10), 1268–1276.
Daley, T.M., Cox, D., 2001. Orbital vibrator seismic source for simultaneous P-and S-wave crosswell acquisition. Geophysics 66, 1471–1480.
Dance, T., 2013. Assessment and geological characterisation of the CO2CRC Otway Project CO2 storage demonstration site: from prefeasibility to injection. Mar. Pet. Geol. 46, 251–269.
Dance, T., LaForce, T., Glubokovskikh, S., Ennis-King, J., Pevzner, R., 2019. Illuminating the geology: post-injection reservoir characterisation of the CO2CRC Otway site. Int. J. Greenh. Gas Control. 86, 146–157.
Davis, T., Landrø, M., Wilson, M., 2019. Geophysics and Geosequestration. Cambridge University Press, Cambridge.
Dillon, P.B., 1990. A comparison between Kirchoff and GRT migration on VSP data. Geophys. Prospect. 38, 757–777.
Dou, S., Ajo-Franklin, J., Daley, T., Robertson, M., Wood, T., Freifeld, B., Pevzner, R., Correa, J., Tertyshnikov, K., Urosevic, M., 2016. Surface Orbital Vibrator (SOV) and Fiber-optic DAS: Field Demonstration of Economical, Continuous-land Seismic Time-lapse Monitoring From the Australian CO2CRC Otway Site, SEG Technical Program Expanded Abstracts 2016. Society of Exploration Geophysicists, pp. 5552–5556.

Dou, S., Wood, T., Ajo-Franklin, J., Robertson, M., Daley, T., Freifeld, B., Pevzner, R., Gurevich, B., 2017. Surface orbital vibrator for permanent seismic monitoring: a signal contents and repeatability appraisal. In: 2017 SEG International Exposition and Annual Meeting. Society of Exploration Geophysicists, Houston, Texas, p. 5.

Egorov, A., Pevzner, R., Bóna, A., Glubokovskikh, S., Puzyrev, V., Tertyshnikov, K., Gurevich, B., 2017. Time-lapse full waveform inversion of vertical seismic profile data: workflow and application to the CO2CRC Otway project. Geophys. Res. Lett. 44, 7211–7218.

Egorov, A., Correa, J., Bóna, A., Pevzner, R., Tertyshnikov, K., Glubokovskikh, S., Puzyrev, V., Gurevich, B., 2018. Elastic full-waveform inversion of vertical seismic profile data acquired with distributed acoustic sensors. Geophysics 83, R273–R281.

Evensen, G., 2009. Data Assimilation: the Ensemble Kalman Filter. Springer Science & Business Media.

Freifeld, B.M., Pevzner, R., Dou, S., Correa, J., Daley, T.M., Robertson, M., Tertyshnikov, K., Wood, T., Ajo-Franklin, J., Urosevic, M., Gurevich, B., 2016. The CO2CRC Otway Project Deployment of a Distributed Acoustic Sensing Network Coupled With Permanent Rotary Sources, 2016, pp. 1–5.

Glubokovskikh, S., Pevzner, R., Dance, T., Caspari, E., Popik, D., Shulakova, V., Gurevich, B., 2016. Seismic monitoring of CO2 geosequestration: CO2CRC Otway case study using full 4D FDTD approach. Int. J. Greenh. Gas Control. 49, 201–216.

Glubokovskikh, S., Pevzner, R., Gunning, J., Dance, T., Shulakova, V., Popik, D., Popik, S., Bagheri, M., Gurevich, B., 2020. How well can time-lapse seismic characterize a small CO2 leakage into a saline aquifer: CO2CRC Otway 2C experiment (Victoria, australia). Int. J. Greenh. Gas Control. 92, 102854.

Hannis, S., 2013. Monitoring the geological storage of CO2. Geological Storage of Carbon Dioxide (CO2). Elsevier, pp. 68–96.

Hartog, A.H., 2017. An Introduction to Distributed Optical Fibre Sensors. CRC Press (Taylor and Francis).

Jenkins, C., 2020. The State of the Art in Monitoring and Verification: an update five years on. Int. J. Greenh. Gas Control. 100, 103118.

Jenkins, C., Marshall, S., Dance, T., Ennis-King, J., Glubokovskikh, S., Gurevich, B., La Force, T., Paterson, L., Pevzner, R., Tenthorey, E., Watson, M., 2017. Validating subsurface monitoring as an alternative option to surface M&V - the CO2CRC's otway stage 3 injection. Energy Procedia 114, 3374–3384.

Jenkins, C., Bagheri, M., Barraclough, P., Dance, T., Ennis-King, J., Freifeld, B., Glubokovskikh, S., Gunning, J., LaForce, T., Marshall, S., 2018. Fit for purpose monitoring-a progress report on the CO2CRC otway stage 3 project. 14th Greenhouse Gas Control Technologies Conference MelboUrne 21–26.

Johnston, D.H., 2013. Practical Applications of Time-lapse Seismic Data. Society of Exploration Geophysicists.

Kragh, E., Christie, P., 2002. Seismic repeatability, normalized rms, and predictability. Lead. Edge 21, 640–647.

Kuvshinov, B.N., 2016. Interaction of helically wound fibre-optic cables with plane seismic waves: interaction of fibre-optic cables. Geophys. Prospect. 64, 671–688.

Lopez, J., Wills, P., La Follett, J., Hornman, J., Potters, J., van Lokven, M., Perkins, C., Trefanenko, C., 2015. Permanent seismic reservoir monitoring for real-time surveillance of thermal EOR at peace River. In: Third EAGE Workshop on Permanent Reservoir Monitoring 2015. European Association of Geoscientists & Engineers, pp. 1–5.

Lüth, S., Bergmann, P., Huang, F., Ivandic, M., Ivanova, A., Juhlin, C., Kempka, T., 2017. 4D seismic monitoring of CO2 storage during injection and post-closure at the Ketzin pilot site. Energy Procedia 114, 5761–5767.

Nakatsukasa, M., Ban, H., Takanashi, M., Kato, A., Worth, K., White, D., 2017. Repeatability of a rotary seismic source at the aquistore CCS site, SEG technical program expanded abstracts 2017. Society of Exploration Geophysicists, pp. 5911–5916.

Oldenburg, C.M., 2018. Are we all in concordance with the meaning of the word conformance, and is our definition in conformity with standard definitions? Greenh. Gases Sci. Technol. 8, 210–214.

Parker, T., Shatalin, S., Farhadiroushan, M., 2014. Distributed acoustic Sensing-A new tool for seismic applications. First Break. 32, 61–69.

Pevzner, R., Urosevic, M., Popik, D., Shulakova, V., Tertyshnikov, K., Caspari, E., Correa, J., Dance, T., Kepic, A., Glubokovskikh, S., Ziramov, S., Gurevich, B., Singh, R., Raab, M., Watson, M., Daley, T., Robertson, M., Freifeld, B., 2017a. 4D surface seismic tracks small supercritical CO2 injection into the subsurface: CO2CRC Otway Project. Int. J. Greenh. Gas Control. 63, 150–157.

Pevzner, R., Urosevic, M., Tertyshnikov, K., Gurevich, B., Shulakova, V., Glubokovskikh, S., Popik, D., Correa, J., Kepic, A., Freifeld, B., Robertson, M., Wood, T., Daley, T., Singh, R., 2017b. Stage 2C of the CO2CRC otway project: seismic monitoring operations and preliminary results. Energy Procedia 114, 3997–4007.

Pevzner, R., Bona, A., Correa, J., Tertyshnikov, K., Palmer, G., Valishin, O., 2018. Optimising DAS VSP Data Acquisition Parameters: Theory and Experiments at Curtin Training Well Facility.

Pevzner, R., Tertyshnikov, K., Sidenko, E., Ricard, L., 2020a. Monitoring Drilling and Completion Operations Using Distributed Acoustic Sensing: CO2CRC Stage 3 Project Case Study, First EAGE Workshop on Fibre Optic Sensing. European Association of Geoscientists & Engineers, pp. 1–5.

Pevzner, R., Urosevic, M., Tertyshnikov, K., AlNasser, H., Caspari, E., Correa, J., Daley, T., Dance, T., Freifeld, B., Glubokovskikh, S., Greenwood, A., Kepic, A., Popik, D., Popik, S., Raab, M., Robertson, M., Shulakova, V., Singh, R., Watson, M., Yavuz, S., Ziramov, S., Gurevich, B., 2020b. - Active surface and borehole seismic monitoring of a small supercritical CO2 injection into the subsurface: experience from the CO2CRC otway project. Chapter 6.1. In: Kasahara, J., Zhdanov, M.S., Mikada, H. (Eds.), Active Geophysical Monitoring, second edition. Elsevier, pp. 497–522.

Popik, S., Pevzner, R., Tertyshnikov, K., Popik, D., Urosevic, M., Shulakova, V., Glubokovskikh, S., Gurevich, B., 2020. 4D surface seismic monitoring the evolution of a small CO2 plume during and after injection: CO2CRC Otway Project study. Explor. Geophys. 1–11.

Roach, L.A., White, D., 2018. Evolution of a deep CO2 plume from time-lapse seismic imaging at the Aquistore storage site, Saskatchewan, Canada. Int. J. Greenh. Gas Control. 74, 79–86.

Shatalin, S.V., Parker, T., Farhadiroushan, M., 2021. High definition seismic and micro-seismic data acquisition using distributed and engineered fiber optic acoustic sensors. Distributed Acoustic Sensing in Geophysics: Methods and Applications. American Geophysical Union. In press.

White, D., 2019. Integrated geophysical characterization and monitoring at the aquistore CO2 storage site. In: Wilson, M., Landrø, M., Davis, T.L. (Eds.), Geophysics and Geosequestration. Cambridge University Press, Cambridge, pp. 257–279.

Wildenborg, T., de Bruin, G., Kronimus, A., Neele, F., Wollenweber, J., Chadwick, A., 2014. Transferring responsibility of CO2 storage sites to the competent authority following site closure. Energy Procedia 63, 6705–6716.

Yavuz, S., Correa, J., Pevzner, R., Freifeld, B., Wood, T., Tertyshnikov, K., Popik, S., Robertson, M., 2019. Assessment of the permanent seismic sources for borehole seismic monitoring applications: CO2CRC Otway Project. Aseg Ext. Abstr. 1–5, 2019.

Yavuz, S., Isaenkov, R., Pevzner, R., Tertyshnikov, K., Yurikov, A., Correa, J., Wood, T., Freifeld, B., 2020. Processing of Continuous Vertical Seismic Profile Data Acquired With Distributed Acoustic Sensors and Surface Orbital Vibrators, 2020, pp. 1–5.